

Multiple copies of orbital angular momentum states through second-harmonic generation in a two-dimensional periodically poled LiTaO₃ crystal

Xinyuan Fang, Dunzhao Wei, Dongmei Liu, Weihao Zhong, Rui Ni, Zhenhua Chen, Xiaopeng Hu, Yong Zhang, S. N. Zhu, and Min Xiao

Citation: *Applied Physics Letters* **107**, 161102 (2015); doi: 10.1063/1.4934488

View online: <http://dx.doi.org/10.1063/1.4934488>

View Table of Contents: <http://scitation.aip.org/content/aip/journal/apl/107/16?ver=pdfcov>

Published by the [AIP Publishing](#)

Articles you may be interested in

[Optical breakdown threshold in nanosecond high repetition second harmonic generation by periodically poled Mg-doped LiTaO₃ crystal](#)

Appl. Phys. Lett. **103**, 091114 (2013); 10.1063/1.4819758

[Second-harmonic generation in a periodically poled congruent LiTaO₃ sample with phase-tuned nonlinear Cherenkov radiation](#)

Appl. Phys. Lett. **100**, 022905 (2012); 10.1063/1.3676440

[Thermal inhibition of high-power second-harmonic generation in periodically poled Li Nb O₃ and Li Ta O₃ crystals](#)

Appl. Phys. Lett. **87**, 131101 (2005); 10.1063/1.2056593

[Second-harmonic generation of green light in periodically poled stoichiometric Li Ta O₃ doped with MgO](#)

J. Appl. Phys. **96**, 7445 (2004); 10.1063/1.1804616

[Second-harmonic generation in two-dimensional periodically poled lithium niobate using second-order quasiphase matching](#)

Appl. Phys. Lett. **82**, 4230 (2003); 10.1063/1.1579856

The advertisement features a white Lake Shore Model 372 cryogenic temperature controller on the left, with a digital display showing '96.837'. To the right is a detailed, close-up view of a cryogenic system's internal components, including a yellow-coated cylindrical chamber and various metal pipes and valves. The Lake Shore CRYOTRONICS logo is in the top right corner.

Precise temperature control
for cryogenic research

Model 372

Lake Shore
CRYOTRONICS

Multiple copies of orbital angular momentum states through second-harmonic generation in a two-dimensional periodically poled LiTaO₃ crystal

Xinyuan Fang,¹ Dunzhao Wei,¹ Dongmei Liu,¹ Weihao Zhong,¹ Rui Ni,¹ Zhenhua Chen,¹ Xiaopeng Hu,¹ Yong Zhang,^{1,a)} S. N. Zhu,¹ and Min Xiao^{1,2,b)}

¹National Laboratory of Solid State Microstructures, College of Engineering and Applied Sciences and School of Physics, Nanjing University, Nanjing 210093, China

²Department of Physics, University of Arkansas, Fayetteville, Arkansas 72701, USA

(Received 31 July 2015; accepted 8 October 2015; published online 21 October 2015)

We experimentally demonstrate multiple copies of optical orbital angular momentum (OAM) states through quasi-phase-matched (QPM) second-harmonic (SH) generation in a 2D periodically poled LiTaO₃ (PPLT) crystal. Since the QPM condition is satisfied by involving different reciprocal vectors in the 2D PPLT crystal, collinear and noncollinear SH beams carrying OAMs of l_2 are simultaneously generated by the input fundamental beam with an OAM of l_1 . The OAM conservation law (i.e., $l_2 = 2l_1$) holds well in the experiment, which can tolerate certain phase-mismatch between the interacting waves. Our results provide an efficient way to obtain multiple copies of the wavelength-converted OAM states, which can be used to enhance the capacity in optical communications. © 2015 AIP Publishing LLC. [<http://dx.doi.org/10.1063/1.4934488>]

It is well known that a vortex beam with a phase dependence of $\exp(i\ell\theta)$ in the azimuthal direction carries orbital angular momentum (OAM).¹ Here, l is defined as the orbital quantum number of photons. OAM of a light beam has been widely applied in optical tweezers,^{2,3} optical manipulation,⁴ and information processing.^{5–8} Recently, the research interests of OAM have been further inspired by the experimental demonstrations that it can significantly enhance the capability of communications.^{9,10} There are several ways to directly generate a light beam with a desired OAM, for example, Q plates, spatial light modulators (SLMs), and diffraction gratings.^{11,12} Recently, due to the increasing demands to imprint OAM onto light beams with different wavelengths (especially the short wavelength), nonlinear optical processes including second-harmonic generation (SHG),^{13–15} sum-frequency generation (SFG),¹⁶ and four-wave mixing¹⁷ have been used to convert the OAM from one light beam to another. Generally, the OAM is conserved during nonlinear optical processes including SHG.^{14,18,19} However, a few exceptions were reported in type-II spontaneous parametric down-conversion processes.^{20,21}

Recently, periodically poled crystals have been introduced to realize highly efficient nonlinear conversion of OAM states through quasi-phase-matching (QPM).^{22,23} Periodically poled nonlinear optical crystals have been extensively used in frequency conversion,²⁴ wave-front engineering,²⁵ and quantum information²⁶ because they can provide reciprocal vectors to realize QPM-enhanced nonlinear optical conversion. In 1998, Berger proposed the concept of nonlinear photonic crystals (i.e., 2D periodically poled nonlinear optical crystals).²⁷ Because of the collinear and non-collinear reciprocal vectors in such nonlinear photonic crystals, numerous interesting phenomena have been discovered including nonlinear Cerenkov radiations,²⁸ conical SHG,²⁹ nonlinear

Talbot self-imaging,³⁰ and so on. In this letter, we experimentally demonstrate that multiple copies of wavelength-converted OAM states can be obtained through SHG in a 2D periodically poled LiTaO₃ (PPLT) crystal.

The sample in our experiment is a squarely poled LiTaO₃ crystal with a size of 10 mm (x) × 5 mm (y) × 0.5 mm (z) (Fig. 1), which was fabricated through a room-temperature electric-field poling technique. The period of the domain structure is $\Lambda = 5.5 \mu\text{m}$, and the duty cycle is about 35%. The experimental setup is shown in Fig. 2. A tunable Ti:Sapphire femtosecond laser serves as the input fundamental field. The pulse width is about 140 fs, and the repetition rate is 80 MHz.

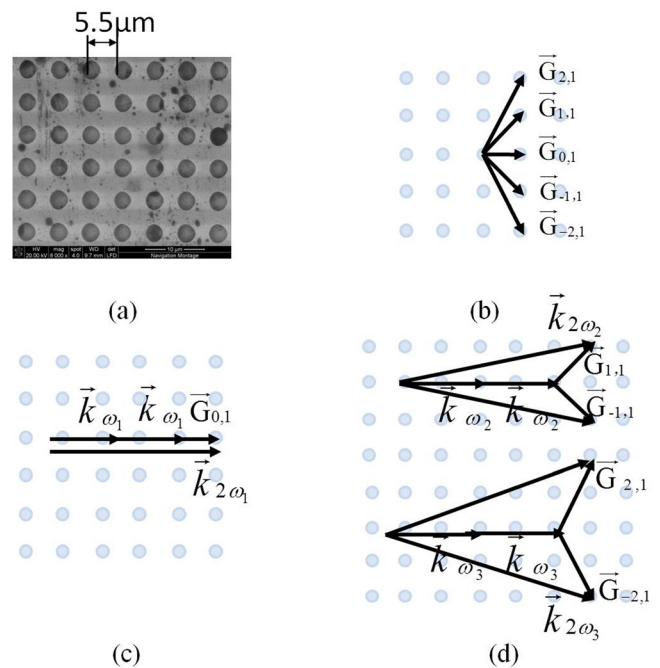


FIG. 1. (a) SEM image of the PPLT sample. (b) Reciprocal lattice vectors. (c) Collinear QPM SHG with $\vec{G}_{0,1}$. (d) Non-collinear QPM SHG with $\vec{G}_{1,1}$, $\vec{G}_{-1,1}$, $\vec{G}_{2,1}$, and $\vec{G}_{-2,1}$.

^{a)}Electronic mail: zhangyong@nju.edu.cn

^{b)}Electronic mail: mxiao@uark.edu

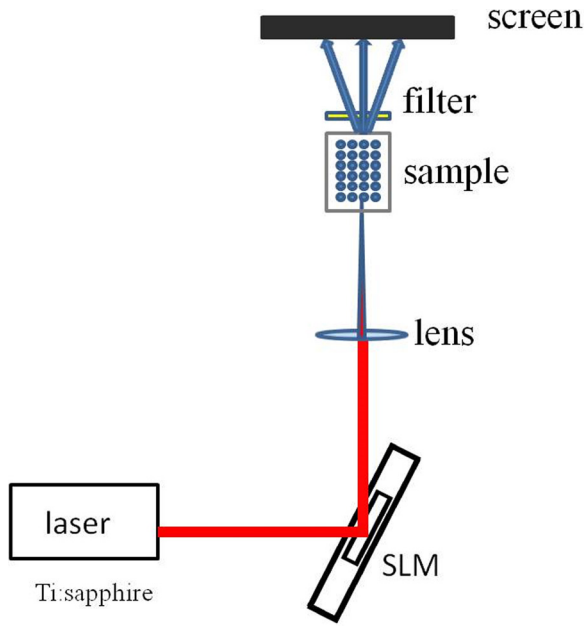


FIG. 2. Schematic of experimental setup.

The wavelength can be continuously tuned from 690 nm to 1050 nm. In the experiment, the input laser is first modulated by a SLM (BNS SN-2840) under a reflection configuration to generate the fundamental beam with a known topological charge. Then, the fundamental wave is focused onto the PPLT slice along the y -axis of the crystal. The polarization of the fundamental light is parallel to the z axis of the crystal. Under this experimental configuration, the involved nonlinear optical coefficient is d_{33} , which is periodically modulated in the PPLT crystal. After filtering out the fundamental beam, the generated SH patterns are projected on a screen located 16 cm away from the end face of the sample. We use a cylindrical lens as a mode converter to analyze the topological charge of the SH wave.³¹ In this method, the topological charge of a vortex beam is equal to the number of the dark stripes of the pattern focused by the cylindrical lens.

When a fundamental beam with a frequency of ω_1 and an OAM of l_1 is frequency-doubled in a PPLT crystal, the energy conservation requires

$$2\omega_1 = \omega_2. \quad (1)$$

Here, ω_2 is the frequency of the SH wave. To realize an efficient conversion, it is necessary to conserve the momentum within the optical fields, which is achieved through QPM in the 2D PPLT crystal. The phase-matching condition can be written as

$$2\vec{k}_\omega + \vec{G}_{m,n} = \vec{k}_{2\omega}, \quad (2)$$

where k_ω and $k_{2\omega}$ are the wave vectors of the fundamental and SH waves, respectively. The reciprocal vector $G_{m,n}$ in a squarely poled LiTaO₃ crystal (Fig. 1(b)) is defined by

$$G_{m,n} = \frac{2\pi\sqrt{m^2 + n^2}}{\Lambda} \quad (3)$$

with the subscripts m and n representing the orders of the reciprocal vectors.²⁷ Its direction can be collinear (for example, $\vec{G}_{0,1}$ in Fig. 1(b)) or non-collinear (for example, $\vec{G}_{1,1}$ in

Fig. 1(b)) with the input fundamental beam. Note that the reciprocal vector can be artificially designed to compensate the phase mismatch between the fundamental and SH waves. It has been experimentally demonstrated that the introduction of OAM in a light beam does not change the QPM condition for SHG.²² This can be attributed to the conservation of OAM during the SHG process, i.e.,

$$2l_1 = l_2, \quad (4)$$

where l_2 is the OAM of the SH wave.

The experimental images on the screen are shown in Fig. 3. The input fundamental beam was imprinted with an OAM of $l_1 = 1, 2,$ and 3 in our experiment. The wavelength is tuned between 900 nm and 950 nm to realize collinear and non-collinear QPM SHG. First, we set the input wavelength to realize collinear QPM by the use of $\vec{G}_{0,1}$. The measured wavelength in the experiment is 945 nm, which is well consistent with the theoretical value of 948 nm deduced from Eq. (2). The corresponding SH image on the screen is shown in Fig. 3(a). The central SH ring results from the collinear SHG involving $\vec{G}_{0,1}$. The corresponding phase-matching configuration is shown in Fig. 1(c). Clearly, there are two non-collinear SH beams in Fig. 3(a). They are generated by the QPM SHG processes involving $\vec{G}_{1,1}$ and $\vec{G}_{-1,1}$ (Fig. 1(d)). The measured exit angle of the non-collinear SH beam is 4.94° , which is in good agreement with the calculated 4.91° from Eq. (2). By using a cylinder lens, the OAMs of the collinear and non-collinear SH beams (Figs. 4(a) and 4(b)) are measured to be $l_2 = 2, 4,$ and 6 , which correspond to the input OAMs of $l_1 = 1, 2,$ and 3 , respectively. Obviously, the OAM conservation law as described in Eq. (4) holds well for both collinear and non-collinear SHG processes. In Fig. 3(a), the intensity of the collinear SH beam with $\vec{G}_{0,1}$ is almost twice that of the non-collinear SHG with $\vec{G}_{1,1}$ or $\vec{G}_{-1,1}$ because high-order reciprocal vectors usually have lower effective nonlinear optical coefficients. When increasing the topological charge of the input

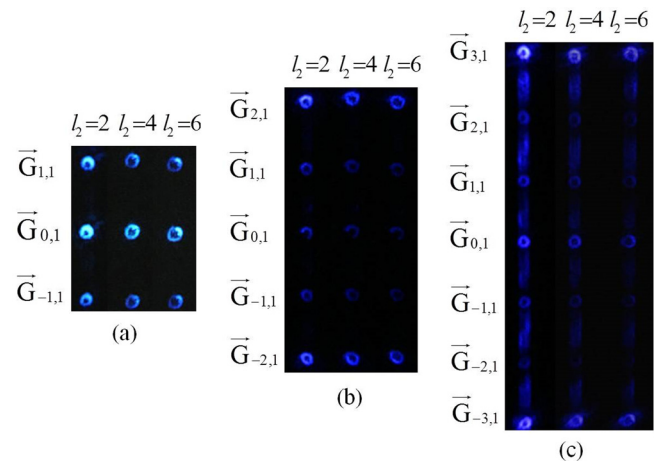


FIG. 3. SH images projected on the screen. (a) At an incident wavelength of 945 nm, collinear and non-collinear QPM SHG processes are simultaneously achieved with the help of $\vec{G}_{1,0}$, $\vec{G}_{1,1}$, and $\vec{G}_{1,-1}$. (b) The phase-matching condition with $\vec{G}_{2,1}$ or $\vec{G}_{-2,1}$ is satisfied at an input wavelength of 926 nm. (c) The fundamental wavelength is 906 nm, which can realize QPM involving $\vec{G}_{3,1}$ and $\vec{G}_{-3,1}$. The topological charges of the generated SH beams and the corresponding reciprocal vectors are also shown in the figures.

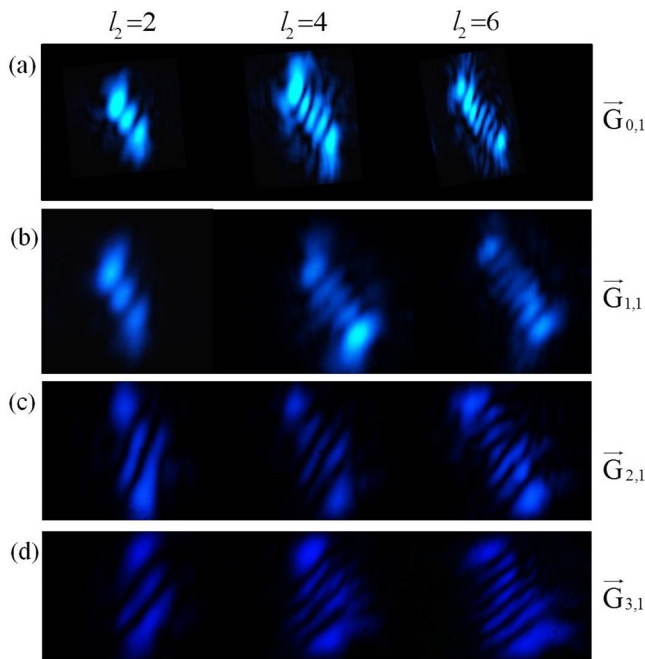


FIG. 4. Measurements of topological charges of the SH beams by using a cylindrical lens. The topological charge can be obtained by counting the number of the dark stripes in the focused patterns. Here, we present the measurements of QPM SH beams. The pump wavelength is 945 nm for (a) and (b), 926 nm for (c), and 906 nm for (d). The corresponding reciprocal vectors are also shown. The measured results of the SH beams under non-perfect QPM conditions are similar, except that their intensities are much lower (not shown here).

beam, the OAM conversion becomes less efficient because high-order OAM modes usually have bigger sizes and lower power densities.

Next, we tune the input wavelength to 926 nm. As shown in Fig. 3(b), the non-collinear SHG process is phase-matched by the reciprocal vectors $\vec{G}_{2,1}$ and $\vec{G}_{-2,1}$. The measured exit angle of the corresponding SH beams is 9.46° while the calculated angle is 9.72° . The OAMs of the SH beams are also doubled in comparison to the input one, as shown in Fig. 4(c). It is interesting to note that the SH beams involving $\vec{G}_{0,1}$, $\vec{G}_{1,1}$, and $\vec{G}_{-1,1}$ can also be observed on the screen. Although their intensities are much lower because the phase mismatches are not perfectly compensated by the reciprocal vectors, their OAMs are still well-defined and conserved. This implies that the OAM conservation law has a certain tolerance for phase-mismatching.

Then, the wavelength is set at 906 nm, which can satisfy the QPM condition for SHG by using the reciprocal vectors $\vec{G}_{3,1}$ and $\vec{G}_{-3,1}$. As shown in Fig. 3(c), the corresponding SH beams are projected onto the screen at an angle of 14.20° . The theoretically calculated exit angle is 14.18° . The OAM of the SH beams can be determined from Fig. 4(d). In Fig. 3(c), one can also see the SH rings resulted from $\vec{G}_{1,0}$, $\vec{G}_{1,1}$, $\vec{G}_{1,-1}$, $\vec{G}_{2,1}$ and $\vec{G}_{-2,1}$, which have much lower intensities due to the non-perfect QPM. Their OAMs are all conserved during the SHG processes. Interestingly, one can find weak SH strips between the well-defined SH rings, which may be attributed to the diffraction from the PPLT structure.³² The OAMs of these SH strips are destroyed or severely distorted because one cannot recognize complete rings in them. One plausible explanation is that the tolerance of OAM

conservation law for phase-mismatching is limited. In our experiments, the OAMs of the SH beams conserve at several special exit angles because the reciprocal vectors in the 2D PPLT crystal can totally or partially compensate for the phase-mismatches between the interacting waves. When the mismatch becomes too large to be compensated by the reciprocal vector, the OAM conversion is destroyed as in the weak SH strips in Fig. 3(c).

In conclusion, we have experimentally demonstrated OAM conversions through SHG in a 2D PPLT crystal. Multiple copies of the SH beams carrying the doubled OAMs are obtained by utilizing the collinear and non-collinear reciprocal vectors in the 2D PPLT crystal. The OAM conservation in non-collinear SHG processes is confirmed. Our experimental results also reveal that the OAM conservation law can tolerate phase-mismatching in a certain range. The 2D PPLT crystal, also known as a nonlinear photonic crystal, can be employed as a potential platform to realize wavelength conversion and multiple copies of OAM states in one device. Potential applications include beam splitter and mode converter in high-capacity optical communications based on OAMs.

This work was supported by the National Basic Research Program of China (Grant Nos. 2012CB921804 and 2011CBA00205), the National Science Foundation of China (Grant Nos. 11274162, 11274165, 61222503, and 11321063), and the New Century Excellent Talents in University and the Priority Academic Program Development of Jiangsu Higher Education Institutions (PAPD).

¹L. Allen, M. W. Beijersbergen, R. J. C. Spreeuw, and J. P. Woerdman, *Phys. Rev. A* **45**, 8185 (1992).

²D. G. Grier, *Nature* **424**, 810 (2003).

³S. Tao, X. C. Yuan, J. Lin, X. Peng, and H. Niu, *Opt. Express* **13**, 7726 (2005).

⁴J. R. Collins and A. Stuart, *J. Opt. Soc. Am.* **60**, 1168 (1970).

⁵A. Mair, A. Vaziri, G. Weihs, and A. Zeilinger, *Nature* **412**, 313 (2001).

⁶A. C. Dada, J. Leach, G. S. Buller, M. J. Padgett, and E. Andersson, *Nat. Phys.* **7**, 677 (2011).

⁷J. T. Barreiro, T. C. Wei, and P. G. B. Kwiat, *Nat. Phys.* **4**, 282 (2008).

⁸D. S. Ding, Z. Y. Zhou, B. S. Shi, and G. C. Guo, *Nat. Commun.* **4**, 2527 (2013).

⁹X. L. Wang, X. D. Cai, Z. E. Su, and J. W. Pan, *Nature* **518**, 516 (2015).

¹⁰Y. Yan, G. Xie, M. P. J. Lavery, H. Huang, N. Ahmed, C. Bao, Y. Ren, Y. Cao, L. Li, Z. Zhao *et al.* *Nat. Commun.* **5**, 4876 (2014).

¹¹N. R. Heckenberg, R. McDuff, C. P. Smith, and A. G. White, *Opt. Lett.* **17**, 221 (1992).

¹²L. Marrucci, C. Manzo, and D. Paparo, *Phys. Rev. Lett.* **96**, 163905 (2006).

¹³K. Dholakia, N. B. Simpson, M. J. Padgett, and L. Allen, *Phys. Rev. A* **54**, R3742 (1996).

¹⁴J. Courtial, K. Dholakia, L. Allen, and M. J. Padgett, *Phys. Rev. A* **56**, 4193 (1997).

¹⁵F. A. Bovino, M. Braccini, M. Giardina, and C. Sibilina, *J. Opt. Soc. Am. B* **28**, 2806 (2011).

¹⁶A. Beržanskis, A. Matijošius, A. Piskarskas, V. Smilgevičius, and A. Stabinis, *Opt. Commun.* **150**, 372 (1998).

¹⁷D. S. Ding, Z. Y. Zhou, B. S. Shi, X. B. Zhou, and G. C. Guo, *Opt. Lett.* **37**, 3270 (2012).

¹⁸A. Vaziri, G. Weihs, and A. Zeilinger, *Phys. Rev. Lett.* **89**, 240401 (2002).

¹⁹G. H. Shao, Z. J. Wu, J. H. Chen, F. Xu, and Y. Q. Lu, *Phys. Rev. A* **88**, 063827 (2013).

²⁰H. H. Arnaut and G. A. Barbosa, *Phys. Rev. Lett.* **85**, 286 (2000).

²¹S. Feng and P. Kumar, *Phys. Rev. Lett.* **101**, 163602 (2008).

²²Z. Y. Zhou, D. S. Ding, Y. K. Jiang, S. Shi, X. S. Wang, B. S. Shi, and G. C. Guo, *Opt. Express* **22**, 20298 (2014).

- ²³S. M. Li, L. J. Kong, Z. C. Ren, Y. Li, C. Tu, and H. T. Wang, *Phys. Rev. A* **88**, 035801 (2013).
- ²⁴S. N. Zhu, Y. Y. Zhu, and N. B. Ming, *Science* **278**, 843 (1997).
- ²⁵Y. Q. Qin, C. Zhang, and Y. Y. Zhu, *Phys. Rev. Lett.* **100**, 063902 (2008).
- ²⁶H. Y. Leng, X. Q. Yu, Y. X. Gong, P. Xu, Z. D. Xie, H. Jin, C. Zhang, and S. N. Zhu, *Nat. Commun.* **2**, 429 (2011).
- ²⁷V. Berger, *Phys. Rev. Lett.* **81**, 4136 (1998).
- ²⁸Y. Zhang, Z. D. Gao, Z. Qi, S. N. Zhu, and N. B. Ming, *Phys. Rev. Lett.* **100**, 163904 (2008).
- ²⁹P. Xu, S. H. Ji, S. N. Zhu, X. Q. Yu, J. Sun, H. T. Wang, J. L. He, Y. Y. Zhu, and N. B. Ming, *Phys. Rev. Lett.* **93**, 133904 (2004).
- ³⁰Y. Zhang, J. Wen, S. N. Zhu, and M. Xiao, *Phys. Rev. Lett.* **104**, 183901 (2010).
- ³¹V. Denisenko, V. Shvedov, A. S. Desyatnikov, D. N. Neshev, W. Krolikowski, A. Volyar, M. Sokin, and Y. S. Kivshar, *Opt. Express* **17**, 23374 (2009).
- ³²S. Juodkazis, E. Gaizauskas, V. Jarutis, J. Reif, S. Matsuo, and H. Misawa, *J. Phys. D: Appl. Phys.* **39**, 50 (2006).